Electronic Supplementary Material (ESI) for ChemComm.

Electronic Supplementary Information

for

$FeNbO_4$ nanochains with five-electron transfer reaction toward high capacity and fast Li storage†

Yingxue Cui,[a,‡] Zixuan Zhou,[a,‡] Sheng Li,[a] Rong Kang,[a] Yun Zhang,[a] Wei Wei,[b] Jiabiao Lian,[a,*] Shanhai Ge[c,*] and Huaming Li[a,*]

[a] Institute for Energy Research, Jiangsu University, Zhenjiang 212013, P. R. China

[b] Supervision Center, Daqing Oilfield Co., Ltd, Daqing 163458, P. R. China

[c] Department of Mechanical Engineering, The Pennsylvania State University, University Park, PA 16802, USA

‡ Y. Cui and Z. Zhou contributed equally to this work.

* Corresponding authors' emails: jblian@ujs.edu.cn (J. Lian), sug13@psu.edu (S. Ge), and lihm@ujs.edu.cn (H. Li)

Experimental section

Synthesis of $FeNbO_4$ nanochains

0.164 g ferric acetylacetonate ($C_{15}H_{21}FeO_6$, AR, Sigma-Aldrich®), 0.250 g niobium oxalate ($C_{10}H_5NbO_{20}$, AR, Sigma-Aldrich®), and 0.475 g polyacrylonitrile (PAN, M_w = 150000, AR, Sigma-Aldrich®) were dissolved in 2 mL, 2 mL, and 5 mL of N,N-dimethylformamide (DMF, AR, Sigma-Aldrich®), respectively, and stirred for 12 h at room temperature. And then, the three solutions were mixed together. After stirring for 12 h, the resulting solution was transferred to a 10 ml plastic syringe containing a 21 G needle for electrospinning (UCALERY, ET-1334). The distance between the aluminum foil collector and the needle tip was 35 cm. A voltage of 18 kV was applied to the needle tip, and the feed rate of the electrospinning solution was 4.8 mm h^{-1}. Finally, the precursor nanofibers were calcined at 800 °C for 2 h at a heating rate of 2 °C min^{-1} in air to obtain $FeNbO_4$ nanochains.

Characterization

The crystal structure of the sample was determined using an X-ray diffractometer (XRD, Brucker D8 Advance) with the Cu Kα radiation in a 2ϑ range of 10°–80° at a scan speed of 5° min^{-1}. The functional groups of the sample was analyzed by Raman spectra (Thermo Fisher DXR) with a 532 nm laser. The morphology, elemental compositions, and microstructure of the material were collected on a transmission electron microscope (TEM, FEI talos F200x G2) equipped with an energy dispersive X-ray spectrometer (EDX, super-x). N_2 adsorption–desorption isotherms of the sample were studied by a gas adsorption analyzer (Micromeritics Tristar II 3020) with a pretreatment temperature of 150 °C. The specific surface area (SSA) and the pore

size distribution was calculated by the Brunauer–Emmett–Teller (BET) method and the Barrett–Joyner–Halenda (BJH) model, respectively. The surface elemental valence states and chemical compositions of the product were analyzed by an X-ray photoelectron spectrometer (XPS, Thermo Scientific K-Alpha) using the Al Kα radiation as the exciting source.

Electrochemical measurements

To evaluate the electrochemical performance of $FeNbO_4$ nanochains, the working electrodes were fabricated by mixing 80 wt.% active materials (the as-prepared $FeNbO_4$), 10 wt.% conductive additives (superconductive carbon black, SCCB, Ketjenblack EC-600JD), and 10 wt.% binder agents (polyvinylidene fluoride, PVDF, AR, Sigma-Aldrich®) in N-methyl-2-pyrrolidone (NMP, AR, Sigma-Aldrich®). After grinding for 1 h, the slurries were coated onto the current collectors (copper foils), followed by drying at 80 °C for 12 h in vacuum. And then, the copper foils were roll-pressed at a pressure of 10 MPa and cut to disks with a diameter of 12 mm. The mass loading of the active materials was about 2.0 mg cm^{-2}. After that, CR2032-type half cells were assembled in an argon-filled glovebox (MIKROUNA, the levels of H_2O and O_2 are below 0.1 ppm), using the resultant working electrodes, lithium foils as the counter and reference electrodes, microporous polypropylene films (Celgard® 2400) as the separators, and 1.0 M $LiPF_6$ in a mixture of ethylene carbonate (EC), dimethyl carbonate (DMC), and ethyl methyl carbonate (EMC) (the volume ratio of EC/DMC/EMC was 1.0 : 1.0 : 1.0, battery grade, Sigma-Aldrich®) as the electrolyte.

The galvanostatic charging/discharging (GCD) and galvanostatic intermittent titration technique (GITT) tests were collected on a Neware battery testing system

(CT-4008). The GCD curves was measured in a potential range of 0.01–3.0 V from 0.1 to 5.0 A g^{-1}. The GITT was conducted with a pulse time of 10 min, a current density of 0.1 A g^{-1}, and a rest interval of 1 h between each pulse. The cyclic voltammetry (CV) and electrochemical impedance spectroscopy (EIS) measurements were performed using a Gamry electrochemical workstation (Interface 1000E). The CV curves were measured within a potential window of 0.01–3.0 V at various scan rates ranging from 0.1–10.0 mV s^{-1}. The EIS was carried out with an AC perturbation of 10 mV and in a frequency range of 100 kHz–10 mHz. For the *in-situ* XRD measurement, an operando electrochemical cell with a beryllium foil as the X-ray window (Beijing Scistar Technology Co. Ltd.) was used. The *in-situ* XRD data was obtained from the aforementioned XRD equipment in a 2ϑ range of 20°–50° at a scan rate of 5° min^{-1} for the initial two GCD cycles measured in a potential window of 0.01–3.0 V (*vs.* Li/Li^+) at a current density of 0.08 A g^{-1}.

Theoretical capacity calculation of $FeNbO_4$

Based on the chemical formula, the redox reaction involved in the lithium-ion intercalation process can be represented as:

$2FeNbO_4 + 10Li^+ + 10e^- \leftrightarrow 2Fe + 3Li_2O + Li_4Nb_2O_5$

To calculate the theoretical specific capacity, we can use the following formula:

Specific capacity (mAh g^{-1}) = F (C mol^{-1}) × n × (1/M) (mol g^{-1}) × (1/3.6) (mAh C^{-1})

where F is the Faraday constant (96485.33 C mol^{-1}), n is the number of electrons involved in the redox reaction (in this case, n = 10), M is the molar mass of $2FeNbO_4$ (425.494 g mol^{-1}). Now, we can calculate the theoretical specific capacity of $FeNbO_4$:

Specific capacity = 96485.33 × 10 × (1/425.494) × (1/3.6) = 629.89 mAh g^{-1}

Calculation of the Li^+ ion diffusion coefficient from GITT measurement

The rate of Li^+ ion diffusion is determined by the change in voltage with time in a GITT test. The D_{Li+} value can be calculated by the following equation:

$$D = \frac{4}{\pi\tau}(\frac{m_B V_M}{M_B S})^2(\frac{\Delta E_s}{\Delta E_\tau})^2$$

where, τ is the duration of the current pulse (s), m_B, M_B, and V_M represent the mass (g), molar mass (g mol^{-1}), and molar volume (cm^3 mol^{-1}) of the active material, S is the electrode-electrolyte interfacial area (cm^2), ΔE_s denotes the steady-state potential change arising from the current pulse (V), and ΔE_τ represents the potential change during the constant current pulse, neglecting the IR drop (V).

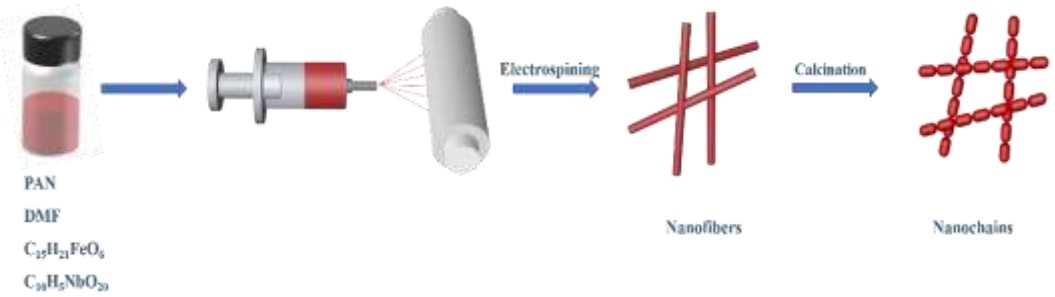

Fig. S1 The schematic illustration of the synthesis process for $FeNbO_4$ nanochains.

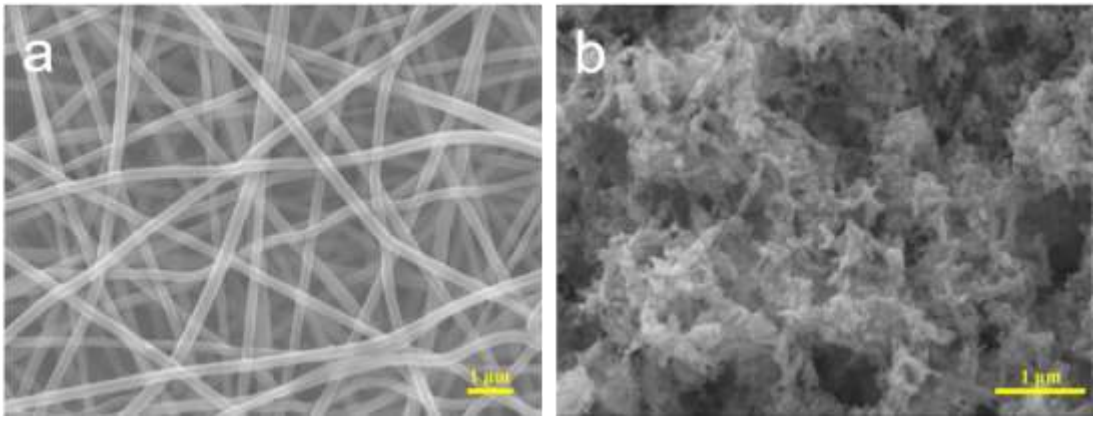

Fig. S2 SEM images of (a) the precursor and (b) $FeNbO_4$ nanochains.

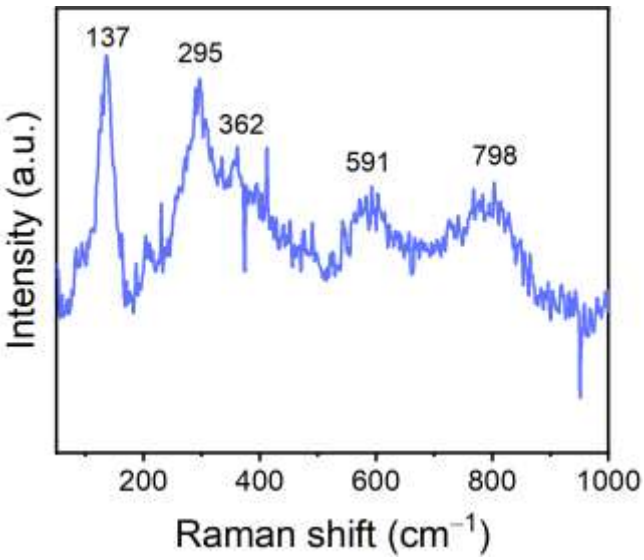

Fig. S3 Raman spectrum of the $FeNbO_4$ nanochains.

The Raman spectrum in Fig. S3 shows five obvious signals. Based on the previously described assignments of the niobate structure, the peaks at 800–300 cm^{-1} can be assigned to the Nb-O stretching bands,[S1] whereas the frequency below 300 cm^{-1} originates from external lattice vibrations.[S2]

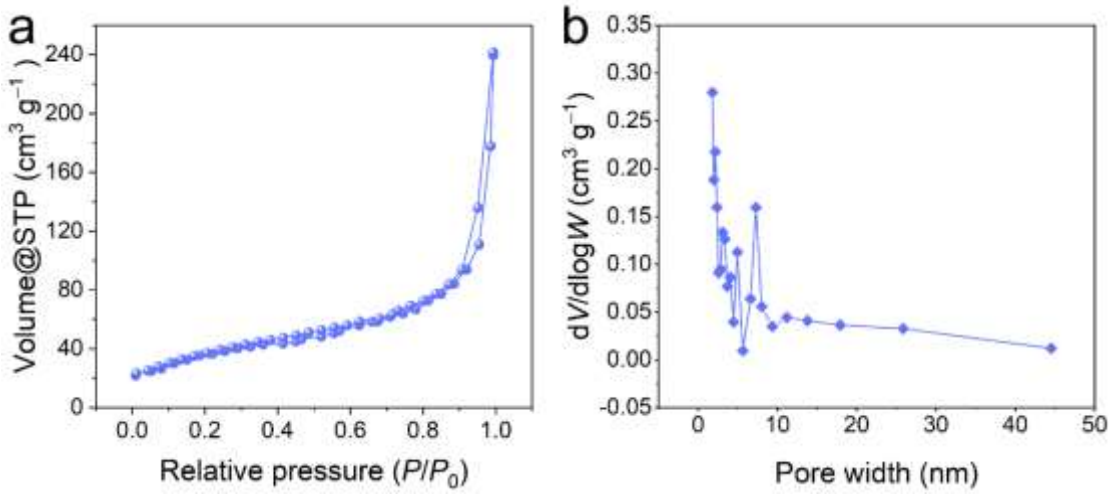

Fig. S4 (a) N_2 adsorption/desorption isotherm and (b) pore size distribution of $FeNbO_4$ nanochains.

The specific surface area of $FeNbO_4$ sample was measured by BET analysis. Nitrogen adsorption-desorption isotherms (Fig. S4a) exhibited typical characteristics of type IV isotherms with H3-type hysteresis loops. The BET-surface area of $FeNbO_4$ sample was determined to be 139.56 m^2 g^{-1}. Such BET surface area is higher than most of the reported data of $FeNbO_4$ materials due to the unique 1D structure. The pore size distribution curve (Fig. S4b) of $FeNbO_4$ indicates that most of the pores are mesopores, which is benefit to the immersion of electrolyte.

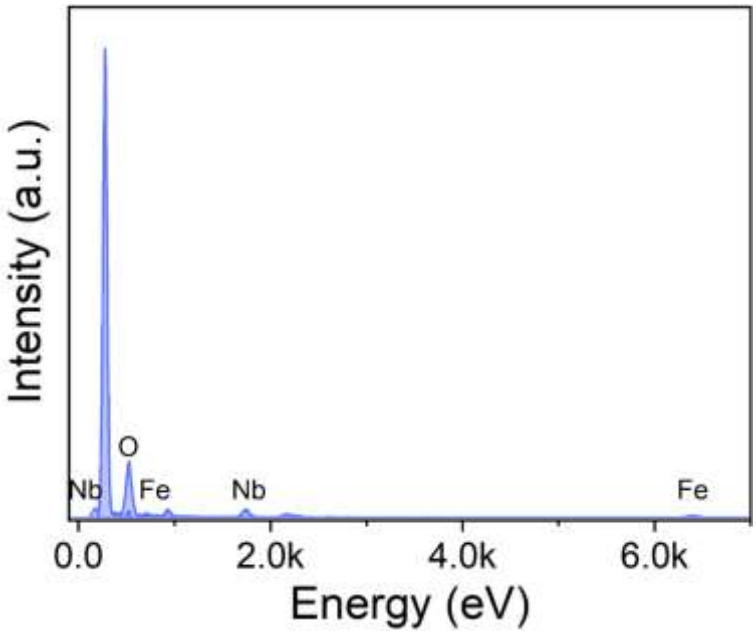

Fig. S5 EDS spectrum of $FeNbO_4$ nanochains.

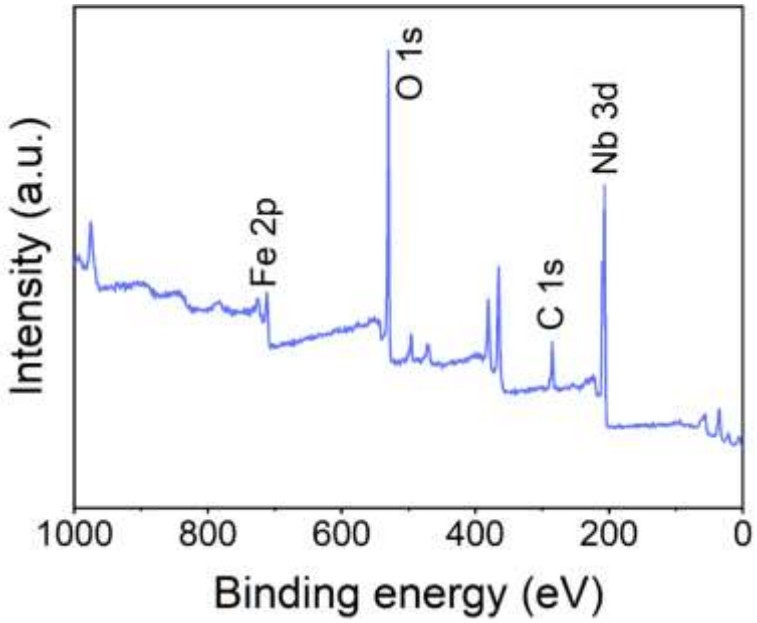

Fig. S6 XPS Survey spectrum of the $FeNbO_4$ nanochains.

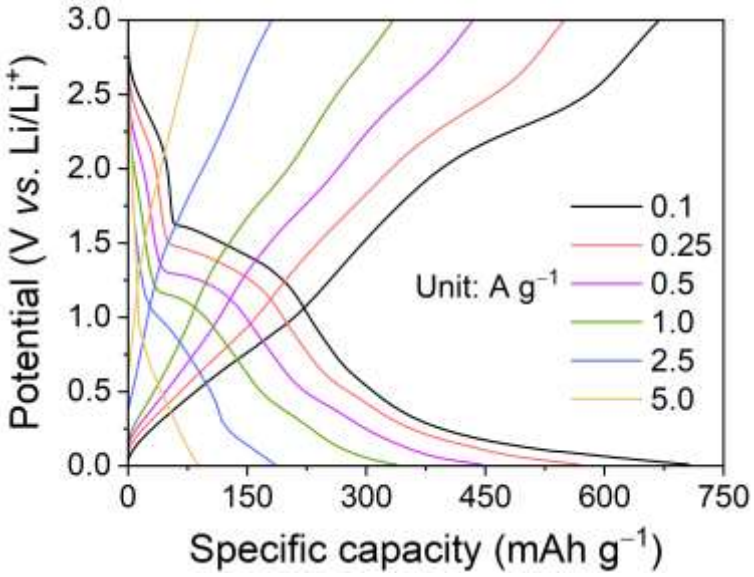

Fig. S7 Charge–discharge profiles of $FeNbO_4$ electrode at different current densities.

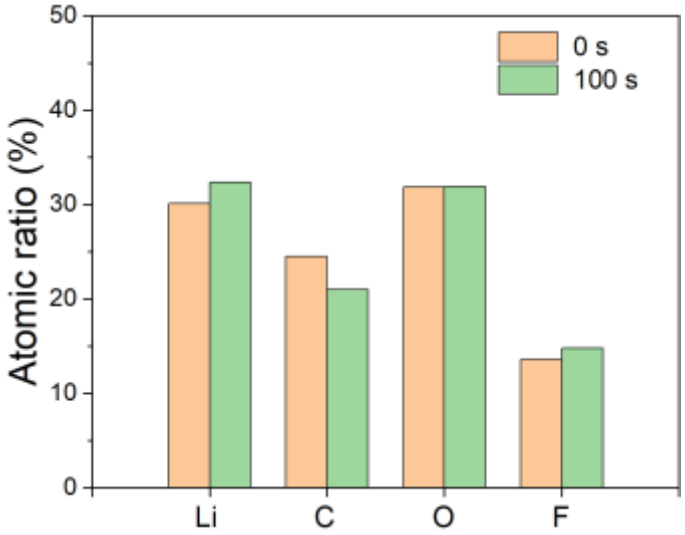

Fig. S8 Atomic ratios of Li, C, O, and F elements in SEI layer obtained from in-depth XPS tests (with and without etching for 100 s).

In-depth XPS tests (with and without etching for 100 s) were carried out to verify the components and their spatial distribution in SEI layers. In general, the atomic concentration ratios of C, Li, O, and F elements at different depths are shown in Fig. S8, in which F content is low compared with the other three elements, demonstrating that the formed SEIs are mainly contributed from the decomposition of the carbonate solvents, in agreement with previous studies. The concentration of C decreases from surface to inter layer, indicating the SEIs are composed of organic-rich outer-layer and inorganic-rich inner-layer, which is consistent with the classic mosaic structure.

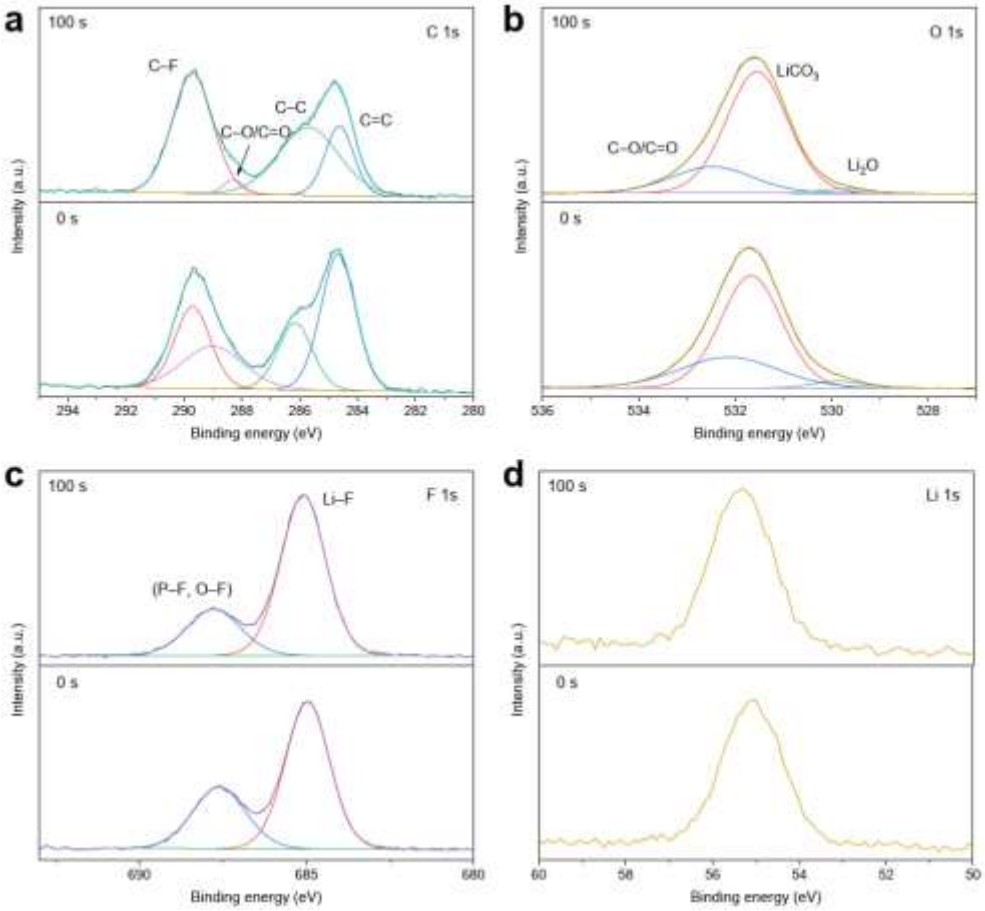

Fig. S9 The XPS spectra of SEI layer with and without etching for 100 s: (a) C 1s, (b) O 1s, (c) F 1s, and (d) Li 1s.

The XPS spectra are deconvoluted to illustrate the SEI composition along the depth, as shown in Fig. S9. The areas of organic species (C=O and C–O) decrease while the area of inorganic species (Li_2CO_3, Li_2O, and LiF) increases with etching, which further proved the SEIs are rich in organic species in the outer layer and rich in inorganic species in the inner layer. The corresponding peaks at 531.7 eV in O 1s spectra (Fig. S9b) and 685.1 eV in F 1s spectra (Fig. S9c) support the presence of Li_2CO_3 and LiF, respectively.

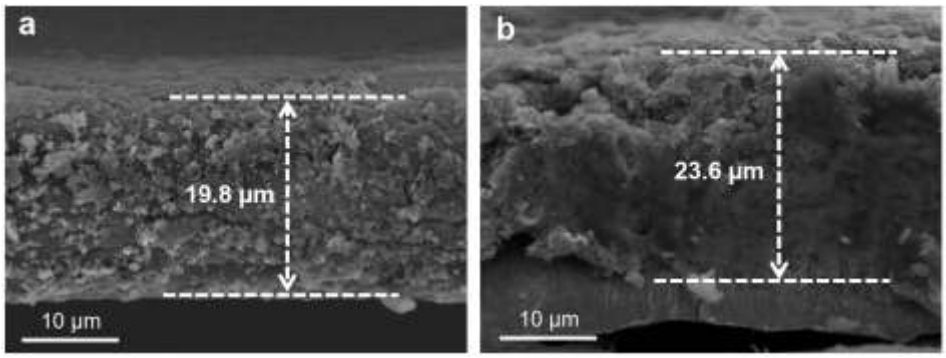

Fig. S10 Cross-sectional SEM images of the $FeNbO_4$ electrode (a) before and (b) after 100 cycles at 0.1 A g^{-1} within the voltage window of 0.01–3.0 V.

We have measured the cross-sectional SEM images of $FeNbO_4$ electrodes before and after cycling analysis. As shown in Fig. S10, the thickness of $FeNbO_4$ electrode before cycle is about 19.8 μm. After cycle, the thickness of the electrode increases to 23.6 μm, indicating a 19.2% volume change of the electrode. Moreover, no apparent cracks can be observed, revealing the positive effects of 1D nanochain structure on cycle performance.

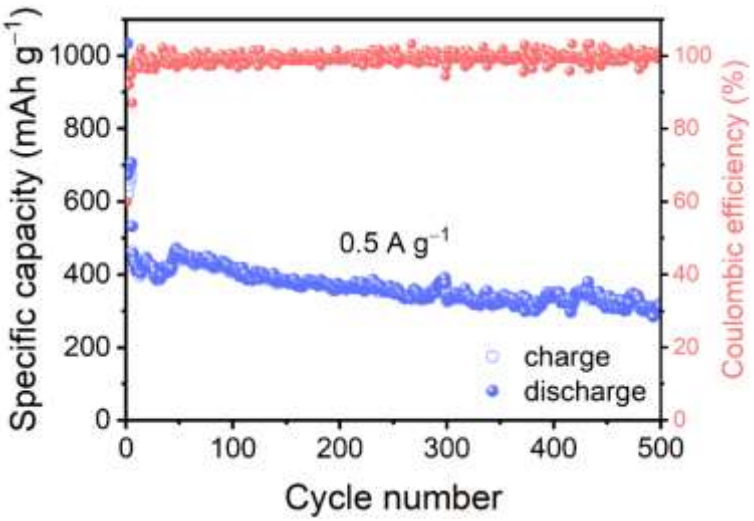

Fig. S11 Long cycle performance of $FeNbO_4$ electrode over 500 cycles at a current density of 0.5 A g^{-1} within the voltage window of 0.01–3.0 V.

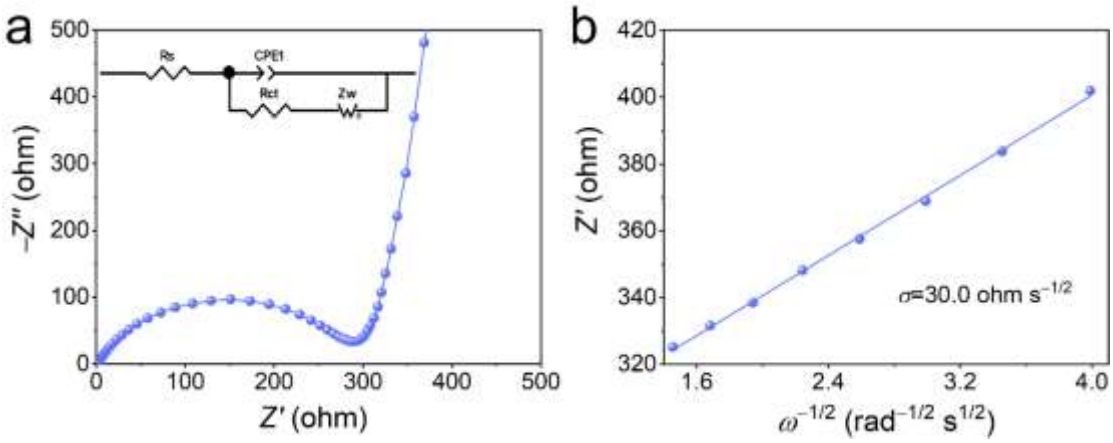

Fig. S12 (a) Nyquist plot at the open circuit potential (inset: the corresponding equivalent circuit model) and (b) calculation of the Warburg coefficient based on the Z'–$\omega^{-1/2}$ plot in the low-frequency region for $FeNbO_4$ electrode.

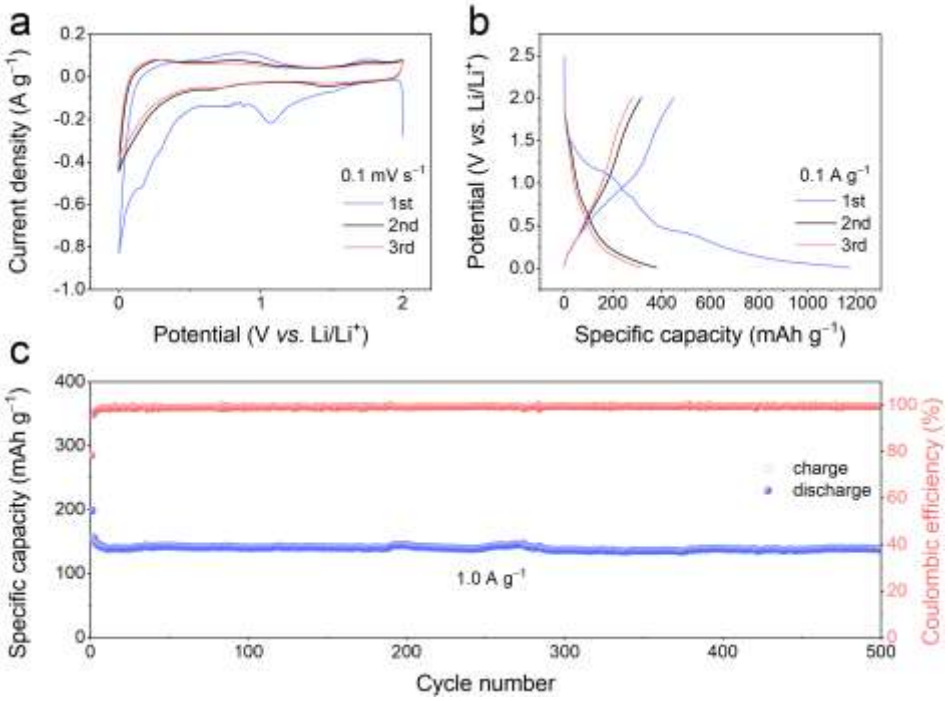

Fig. S13 Electrochemical performance of the $FeNbO_4$ electrode within the voltage window of 0.01–2.0 V. (a) Initial three CV curves at 0.1 mV s^{-1}. (b) Initial three GCD profiles at 0.1 A g^{-1}. (c) Cycle performance at 1.0 A g^{-1}.

To discuss how the capacity changes as the voltage window varies, we have examined the Li^+ storage behavior of $FeNbO_4$ within the potential window of 0.01–2.0 V. Fig. S13a and S13b show the initial three CV curves at 0.1 mV s^{-1} and GCD profiles at 0.1 A g^{-1} of $FeNbO_4$ electrode within the potential window of 0.01–2.0 V, respectively. $FeNbO_4$ shows a discharge capacity of ~400 mAh g^{-1}, which is lower than that in the voltage window of 0.01–3.0 V. The cycling test of $FeNbO_4$ at 1.0 A g^{-1} over 500 cycles is shown in Fig. S13c, exhibiting ultrastable cycle performance with a capacity of 142 mAh g^{-1} after 500 cycles. Although the capacity decreases as compared with that in the voltage window of 0.01–3.0 V, the cycle stability is still satisfactory for practical utility.

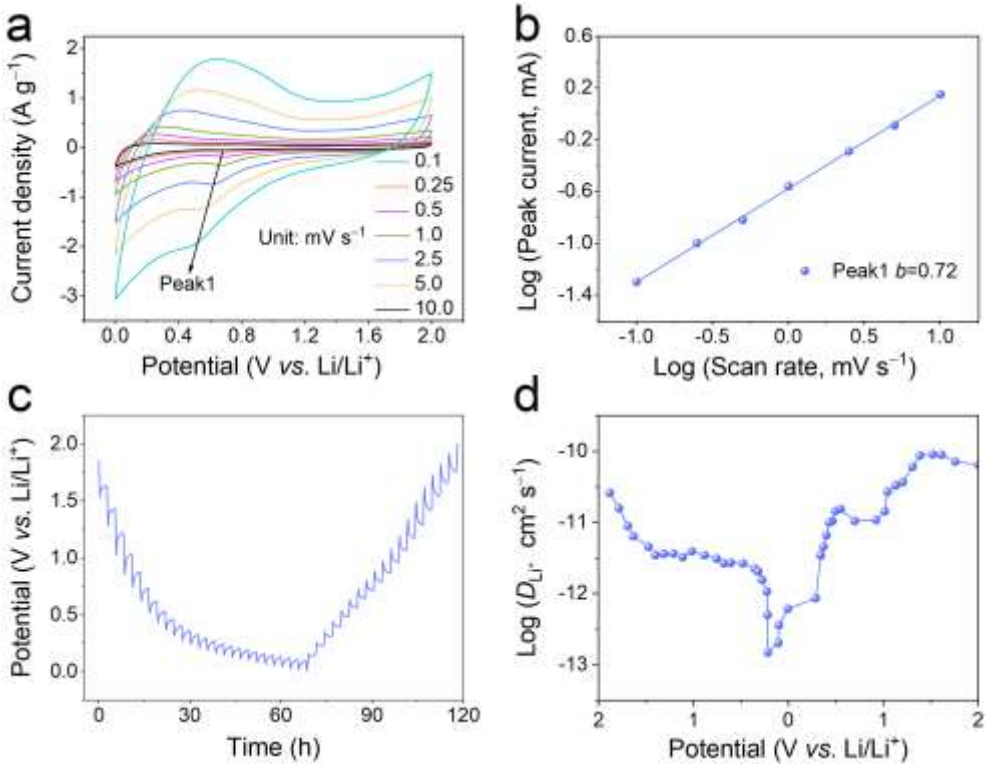

Fig. S14 Reaction kinetic analysis of the $FeNbO_4$ electrode within the voltage window of 0.01–2.0 V. (a) CV curves at different scan rates. (b) Relationship between log(*i*) and log(*v*) derived from the CV curves in (a). (c) GITT profile at 0.1 A g^{-1}. (d) Calculated lithium diffusion coefficient (D_{Li^+}).

The electrochemical reaction kinetics of $FeNbO_4$ nanochains are estimated by CV tests (Fig. S14a) at different scan rates from 0.1 to 10.0 mV s^{-1}. The calculated *b* value (Fig. S14b) based on the cathodic peak 1 is 0.72, revealing that $FeNbO_4$ displays both diffusion and intercalation pseudocapacitive storage. The GITT results (Fig. S14c and S14d) show that the D_{Li+} values $FeNbO_4$ within 0.01–2.0 V are located at a range of 10^{-10} to 10^{-13} cm^2 s^{-1}, which is close to the D_{Li+} values at 0.01–3.0 V. The high *b* value and D_{Li+} values reveal the fast reaction kinetics of $FeNbO_4$ at 0.01–2.0 V.

Table S1 Electrochemical performance of previously reported Fe-Nb based oxides and other TM-Nb based oxides for lithium-ion batteries.

Anode[Ref.]	Morphology	Potential window (V)	Rate capability	Cycle performance
$FeNbO_4$[This work]	**nanochains**	**0.01–3.0**	**661 mAh g^{-1} at 0.1 A g^{-1} 119 mAh g^{-1} at 5.0 A g^{-1}**	**319 mAh g^{-1} at 0.5 A g^{-1} over 500 cycles**
$FeNbO_4$[S3]	bulk	0.001–3.0	120 mAh g^{-1} at 17.0 mA g^{-1} 50 mAh g^{-1} at 170.0 mA g^{-1}	45 mAh g^{-1} at 170.0 mA g^{-1} over 100 cycles
$FeNbO_4$[S3]	nanoparticles	0.001–3.0	420 mAh g^{-1} at 17.0 mA g^{-1} 220 mAh g^{-1} at 170.0 mA g^{-1}	200 mAh g^{-1} at 170.0 mA g^{-1} over 100 cycles
$FeNbO_4$[S4]	nanorod	0.001–3.0	531 mAh g^{-1} at 0.02 A g^{-1} 110 mAh g^{-1} at 1.0 A g^{-1}	358 mAh g^{-1} at 0.1 A g^{-1} over 100 cycles
$FeNbO_4$[S4]	bulk	0.001–3.0	302 mAh g^{-1} at 0.02 A g^{-1} 45 mAh g^{-1} at 1.0 A g^{-1}	125 mAh g^{-1} at 0.1 A g^{-1} over 100 cycles
$FeNbO_4$[S5]	nanospheres	0.01–3.0	288 mAh g^{-1} at 37.2 mA g^{-1} 106 mAh g^{-1} at 186.0 mA g^{-1}	200 mAh g^{-1} at 74.4 mA g^{-1} over 20 cycles
$FeNbO_4$[S5]	bulk	0.01–3.0	152 mAh g^{-1} at 37.2 mA g^{-1} 74 mAh g^{-1} at 186.0 mA g^{-1}	-
$CrNbO_4$[S6]	nanoparticles	0.001–3.0	232.4 mAh g^{-1} at 32.0 mA g^{-1} 137.1 mAh g^{-1} at 160 mA g^{-1}	210 mAh g^{-1} at 16.0 mA g^{-1} over 50 cycles
$CrNbO_4$[S6]	bulk	0.001–3.0	150 mAh g^{-1} at 32.0 mA g^{-1} 50 mAh g^{-1} at 160.0 mA g^{-1}	89 mAh g^{-1} at 16.0 mA g^{-1} over 50 cycles
$CoNb_2O_6$/rGO[S7]	nanospheres	0.01–3.0	450 mAh g^{-1} at 0.1 A g^{-1} 48 mAh g^{-1} at 20.0 A g^{-1}	218.9 mAh g^{-1} at 1.0 A g^{-1} over 1000 cycles
$CoNb_2O_6$[S8]	nanoparticles	0.01–3.0	350 mAh g^{-1} at 0.1 A g^{-1} 50 mAh g^{-1} at 5.0 A g^{-1}	150 mAh g^{-1} at 2.0 A g^{-1} over 1000 cycles
$NiNb_2O_6$[S9]	nanoparticles	0.01–3.0	429.5 mAh g^{-1} at 0.2 A g^{-1} 92.5 mAh g^{-1} at 20.0 A g^{-1}	320.9 mAh g^{-1} at 2.0 A g^{-1} over 500 cycles

Supplementary References

S1 I.-S. Cho, S. Lee, J. H. Noh, G. K. Choi, H. S. Jung, D. W. Kim and K. S. Hong, *J. Phys. Chem. C*, 2008, **112**, 18393–18398.

S2 R. Babu, S. Kelkar, V. Kashid, S. N. Achary, H. G. Salunkee and N. M. Gupta, *RSC Adv.*, 2014, **4**, 33435–33445

S3 T. Wang, S. Shi, F. Kong, G. Yang, B. Qian and F. Yin, *Electrochim. Acta*, 2016, **203**, 206-212.

S4 T. Wang, T. Ge, S. Shi, M. Wu and G. Yang, *J. Alloys Compd.*, 2018, **740**, 7-15.

S5 H.-W. Shim, I.-S. Cho, K. S. Hong, A.-H. Lim and D.-W. Kim, *J. Ceram. Soc. Jpn.*, 2012, **120**, 82-85.

S6 F. Kong, G. Jiao, J. Wang, S. Tao, Z. Han, Y. Fang, G. Yang, L. Zhan and Bin Qian, *Mater. Lett.*, 2017, **196**, 335-338.

S7 P. Chen, C. Zhang, B. Jie, H. Zhang, K. Zhang and Y. Song, *J. Alloys Compd.*, 2022, **908**, 164542.

S8 S. Zhao, T. Chen, H. Li, Y. Liu, M. Huang, C. Xu, Y. Cui, G. Li, J. Lian and Y. Wang, *Chem. Eng. J.*, 2023, **472**, 145115.

S9 S. Zhao, J. Lian, S. Zhang, Y. Cui, G. Li, Y. Wang and H. Li, *Chem. Eng. J.*, 2023, **461**, 141997.